An Efficient 1-D Periodic Boundary Integral Equation Technique to Analyze Radiation onto Straight and Meandering Microstrip Lines

Dries Vande Ginste[1], *Member, IEEE,* Hendrik Rogier[1], *Senior Member, IEEE,* Daniël De Zutter[1], *Fellow, IEEE*

***Abstract*— A modeling technique to analyze the radiation onto arbitrary 1-D periodic metallizations residing on a microstrip substrate is presented. In particular, straight and meandering lines are being studied. The method is based on a boundary integral equation (BIE), more specifically on a mixed potential integral equation (MPIE), that is solved by means of the Method of Moments (MoM). A plane wave excites the microstrip structure, and according to the Floquet-Bloch theorem, the analysis can be restricted to one single unit cell. Thereto, the MPIE must be constructed using the pertinent 1-D periodic layered medium Green's functions. Here, these Green's functions are obtained in closed form by invoking the Perfectly Matched Layer (PML)-paradigm. The proposed method is applied to assess the radiation onto (i) a semi-infinite plate, (ii) a straight microstrip line, and (iii) a serpentine delay line. These three types of examples clearly illustrate and validate the method. Also, its efficiency, compared to a previously developed fast microstrip analysis technique, is demonstrated.**

***Index Terms*— Green's function, periodic structure, Perfectly Matched Layer, electromagnetic radiation, integral equation, Method of Moments, microstrip structure, meandering lines**

I. Introduction

Frequency selective surfaces [1], [2], metamaterials [3], electromagnetic bandgap and defected ground structures [4], [5], leaky wave antennas [6], antenna arrays [7], and wire-medium screens [8] are some typical examples of structures that can exhibit a one-dimensional (1-D), a two-dimensional (2-D), or a three-dimensional (3-D) periodicity. Also, a 1-D periodic meandering character of interconnect structures can be exploited (or introduced) to make them stretchable [9] or to use them as delay lines [10]. Often, techniques to analyze the electromagnetic properties of periodic structures with an infinite extent are based on the Floquet-Bloch theorem, allowing to consider one single representative unit cell. When constructing boundary integral equation (BIE) techniques, the pertinent *periodic* Green's function of the background medium under consideration needs to be computed in order to determine the unknown fields or current distributions within this unit cell. Upon knowledge of the Green's function, the BIE can be solved by the Method of Moments (MoM) [11]. An overview of techniques is provided in [12]. Additionally, a new interesting method based on fast periodic interpolations is reported in [13].

[1] Electromagnetics Group, Department of Information Technology, Ghent University, Sint-Pietersnieuwstraat 41, 9000 B-Gent, Belgium. E-mail: dries.vande.ginste@intec.UGent.be, Tel.: +32 9 264 33 54, Fax: +32 9 264 99 69.

Many structures reside in a layered dielectric background medium. Hence, layered medium periodic Green's functions and BIE-MoM based solution schemes leveraging these Green's functions are of particular interest. Unfortunately, cumbersome Sommerfeld-type integrals then have to be dealt with, leading to a time-consuming numerical evaluation of the layered medium Green's functions. The evaluation of the Sommerfeld-integrals is a challenging research topic. In [14] an efficient sum of inverse Fourier transforms is constructed to tackle the Sommerfeld-integrals. In [15] a novel application of the Perfectly Matched Layer (PML) has been presented. Whereas the PML was originally conceived to serve as an absorbing boundary condition to terminate the simulation domain in finite element and finite difference based full-wave solvers, in [15] the PML is used to construct *closed-form* expressions of layered medium Green's functions. Apart from a rapid evaluation of the pertinent Green's functions, these closed-from expressions can also be used, for example, to construct Fast Multipole Methods [16]–[18]. In [19] the PML-paradigm was applied to conceive 3-D layered medium 1-D *periodic* Green's functions. As the PML-based periodic Green's functions can be constructed in an elegant and natural way, it is very beneficial to implement them within a BIE-MoM scheme. This technique has been successfully applied in [12] to analyze the scattering and radiation from/by 1-D periodic microstrip antenna arrays. However, the technique presented in [12] can only be applied to antenna arrays as a completely arbitrary shape of the metallization within one unit cell was not allowed. In contrast, the method presented in this paper allows to rapidly evaluate the current density on arbitrary 1-D periodic microstrip metallizations, illuminated by a plane wave. In particular, lines with a 1-D periodicity, such as serpentine delay lines [10], are considered. The analysis of such structures is of specific importance to assess possible electromagnetic interference (EMI) issues.

This paper is organized as follows. In Section II the formalism is presented. The PML-paradigm and the periodic Green's functions resulting from it are briefly revisited and the implementation of the PML-based Green's functions in a BIE-MoM scheme is presented. Special attention is devoted to the construction of the MoM in order to allow a continuous current flow across the unit cell's borders. The formalism is validated and illustrated in Section III by considering the radiation onto (i) a large, semi-infinite, perfect electrically conducting (PEC) plate, (ii) a straight microstrip line, and (iii) a serpentine delay line. Conclusions are summarized in Section IV.

In the sequel, all sources and fields are assumed to be time-harmonic with angular frequency ω and time dependencies $e^{j\omega t}$ are suppressed. Also, transverse to z restrictions of vectors $\mathbf{v}$ are denoted $\check{\mathbf{v}} \equiv v_x\hat{\mathbf{x}} + v_y\hat{\mathbf{y}} = -\hat{\mathbf{z}} \times [\hat{\mathbf{z}} \times \mathbf{v}]$; here $\hat{\mathbf{x}}$, $\hat{\mathbf{y}}$, and $\hat{\mathbf{z}}$ are unit Cartesian vectors.

II. Description of the technique

A. Geometry

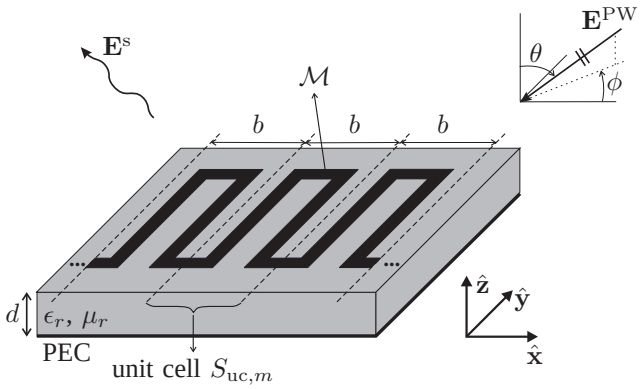

Fig. 1: A 1-D periodic microstrip structure, i.e. a meandering line, illuminated by a plane wave $\mathbf{E}^{\mathrm{PW}}$.

Consider the microstrip geometry of Fig. 1. It consists of a substrate of thickness d, relative permittivity ϵ_r, and relative permeability μ_r, that resides on a perfect electrically conducting (PEC) ground plate. At the substrate-air interface $z = d$, a PEC metallization $\mathcal{M}$ is placed. This metallization exhibits a 1-D periodicity with period b along the x-direction. The mth unit cell is denoted $S_{\mathrm{uc},m} = \{\boldsymbol{\rho} \equiv x\hat{\mathbf{x}} + y\hat{\mathbf{y}} + d\hat{\mathbf{z}} : mb \leq x < (m+1)b\,,\ -\infty < y < \infty\}$, $m \in \mathbb{Z}$. In contrast to our previous work [12], which only allowed the analysis of antenna arrays, here the metallization extends across the borders of the unit cells, allowing a continuous current flow in the x-direction. A plane wave $\mathbf{E}^{\mathrm{PW}}(\mathbf{r} \equiv x\hat{\mathbf{x}}+y\hat{\mathbf{y}}+z\hat{\mathbf{z}}) = \mathbf{E}_0 e^{-jk_0\hat{\mathbf{k}}\cdot\mathbf{r}}$ illuminates the structure. Here, $k_0 = \omega/c$ is the free-space wavenumber, with $c = 1/\sqrt{\epsilon_0\mu_0}$ the speed of light in vacuum. The unit vector $\hat{\mathbf{k}} = -\sin\theta\cos\phi\,\hat{\mathbf{x}} - \sin\theta\sin\phi\,\hat{\mathbf{y}} - \cos\theta\,\hat{\mathbf{z}}$ determines the plane wave's spherical angles of incidence θ and ϕ.

B. 1-D periodic BIE-MoM Formalism

Due to the plane wave, an incident field $\mathbf{E}^{\mathrm{i}}(\mathbf{r})$ is present, which induces an unknown current density $\check{\mathbf{J}}(\boldsymbol{\rho})$ on the metallization. In turn, a scattered field $\mathbf{E}^{\mathrm{s}}(\mathbf{r})$ is produced. A BIE, and more specifically a mixed potential integral equation (MPIE), is now constructed by demanding that the total tangential electric field, i.e. $\check{\mathbf{E}}^{\mathrm{t}}(\mathbf{r}) = \check{\mathbf{E}}^{\mathrm{i}}(\mathbf{r}) + \check{\mathbf{E}}^{\mathrm{s}}(\mathbf{r})$, vanishes at the metallization $\mathcal{M}_{\mathrm{uc},m} = \mathcal{M} \cap S_{\mathrm{uc},m}$ that resides within the mth unit cell:

$$\check{\mathbf{E}}^{\mathrm{i}}(\boldsymbol{\rho}) = j\omega \iint_{\mathcal{M}_{\mathrm{uc},m}} G_A^{\mathrm{per}}(\boldsymbol{\rho}|\boldsymbol{\rho}')\check{\mathbf{J}}(\boldsymbol{\rho}')\,d\boldsymbol{\rho}' - \frac{1}{j\omega}\check{\boldsymbol{\nabla}} \iint_{\mathcal{M}_{\mathrm{uc},m}} G_V^{\mathrm{per}}(\boldsymbol{\rho}|\boldsymbol{\rho}')(\check{\boldsymbol{\nabla}}' \cdot \check{\mathbf{J}}(\boldsymbol{\rho}'))\,d\boldsymbol{\rho}', \quad \forall \boldsymbol{\rho} \in \mathcal{M}_{\mathrm{uc},m}, \tag{1}$$

with $\check{\boldsymbol{\nabla}} = \frac{\partial}{\partial x}\hat{\mathbf{x}} + \frac{\partial}{\partial y}\hat{\mathbf{y}}$. The pertinent 1-D periodic Green's functions $G_A^{\mathrm{per}}(\boldsymbol{\rho}|\boldsymbol{\rho}')$ and $G_V^{\mathrm{per}}(\boldsymbol{\rho}|\boldsymbol{\rho}')$ will be discussed later (see Section II-C). The MPIE (1) is solved by the MoM. Thereto, the metallization is approximated by a rectilinear mesh, as indicated in Fig. 2 (where the depicted metallization $\mathcal{M}_{\mathrm{uc},m}$ is chosen to be a rectangle of length b and width w). The unknown current density $\check{\mathbf{J}}(\boldsymbol{\rho})$ is expanded

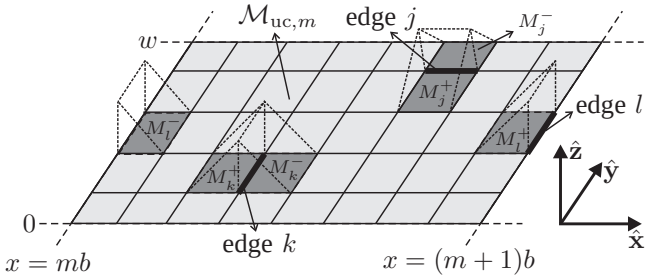

Fig. 2: Discretization of the metallization within the mth unit cell into a rectilinear mesh and some corresponding vector rooftop basis functions. In this example, the metallization $\mathcal{M}_{\mathrm{uc},m}$ is a rectangle of length b and width w.

into a set of x- and y-oriented vector rooftop basis functions [20]. The support M_j of each basis function comprises two patches M_j^- and M_j^+ that are joined by the mesh's jth edge. As indicated in Fig. 2, three cases can be distinguished:

1) the edge is an x-oriented edge (e.g., edge j in Fig. 2);
2) the edge is a y-oriented edge that does not reside on the borders $x = mb$ or $x = (m+1)b$ of the unit cell (e.g., edge k in Fig. 2);
3) the edge is a y-oriented edge that resides on the border $x = (m+1)b$ of the unit cell (e.g., edge l in Fig. 2). In this case, it is noticed that, within this unit cell, the support M_l^- for the falling part of the vector rooftop function does not reside next to the support M_l^+.

Edges residing on the border $x = mb$ have to be neglected, i.e. no basis function should be introduced for these edges, as otherwise the matrix system (see further) would become overdetermined. This is because it is required that the current density is periodic, apart from a phase difference ψ, as follows:

$$\check{\mathbf{J}}(\boldsymbol{\rho} + b\hat{\mathbf{x}}) = \check{\mathbf{J}}(\boldsymbol{\rho})e^{j\psi}, \tag{2}$$

with

$$\psi = -b\,k_0 \sin\theta\cos\phi. \tag{3}$$

The property (2) is a direct consequence of the Floquet-Bloch theorem. To enforce this property, first, the support M_l of the rooftop basis functions corresponding to edges that reside on the border $x = (m+1)b$ consists of a first cell M_l^+ that is adjacent to this border (rising flank of the function) and a second cell M_l^- that is adjacent to the border $x = mb$ (falling flank of the function) (see Fig. 2). Next, assuming that there are N edges after discretization of the metallization, the unknown current density is expanded as follows:

$$\check{\mathbf{J}}(\boldsymbol{\rho}) = \sum_{j=1}^{N} I_j \check{\mathbf{w}}_j^{\mathrm{per}}(\boldsymbol{\rho}). \tag{4}$$

For edges that are not on the border $x = (m+1)b$, in the above expansion (4) the basis functions $\check{\mathbf{w}}_j^{\mathrm{per}}(\boldsymbol{\rho})$ are the classic well-known rooftop basis functions. For edges that are on the border $x = (m+1)b$, the falling flank of the rooftop function (e.g., with support M_l^- in Fig. 2) is subjected to a phase shift so that the requirement (2) is fulfilled. A similar procedure was applied in [21] to develop a 2-D hybrid finite-element (FE)/BIE solver for periodic absorbers. For completeness, note that this procedure can also be applied using Rao-Wilton-Glisson (RWG) basis functions, as described in [14]. Inserting (4) into the MPIE (1) and applying a Galerkin testing procedure [22] results in an $N \times N$ linear system in the unknown expansion coefficients I_j, $j = 1, \ldots, N$:

$$\mathbf{V} = \overline{\mathbf{Z}} \cdot \mathbf{I}. \tag{5}$$

The N-vector $\mathbf{V}$, with elements V_i, $i = 1, \ldots, N$, and the $N \times N$ matrix $\overline{\mathbf{Z}}$, with elements Z_{ij}, $i = 1, \ldots, N$, $j = 1, \ldots, N$, are given by:

$$V_i = \iint_{M_i} \check{\mathbf{E}}^{\mathrm{i}}(\boldsymbol{\rho}) \cdot \check{\mathbf{w}}_i^{\mathrm{per}}(\boldsymbol{\rho})\, d\boldsymbol{\rho}, \tag{6}$$

$$\begin{aligned} Z_{ij} = {} & j\omega \iint_{M_i} \iint_{M_j} G_A^{\mathrm{per}}(\boldsymbol{\rho}|\boldsymbol{\rho}') \left(\check{\mathbf{w}}_i^{\mathrm{per}}(\boldsymbol{\rho}) \cdot \check{\mathbf{w}}_j^{\mathrm{per}}(\boldsymbol{\rho}')\right) d\boldsymbol{\rho}'\, d\boldsymbol{\rho} \\ & + \frac{1}{j\omega} \iint_{M_i} \iint_{M_j} G_V^{\mathrm{per}}(\boldsymbol{\rho}|\boldsymbol{\rho}') (\check{\boldsymbol{\nabla}} \cdot \check{\mathbf{w}}_i^{\mathrm{per}}(\boldsymbol{\rho})) \\ & \qquad \times (\check{\boldsymbol{\nabla}}' \cdot \check{\mathbf{w}}_j^{\mathrm{per}}(\boldsymbol{\rho}'))\, d\boldsymbol{\rho}'\, d\boldsymbol{\rho}. \end{aligned} \tag{7}$$

The linear system (5) can be solved by means of direct or iterative schemes.

C. 1-D periodic Green's functions

Upon knowledge of the 1-D periodic layered medium Green's functions $G_A^{\mathrm{per}}(\boldsymbol{\rho}|\boldsymbol{\rho}')$ and $G_V^{\mathrm{per}}(\boldsymbol{\rho}|\boldsymbol{\rho}')$ for the magnetic vector potential and for the electric scalar potential respectively, the MoM system (5) is fully determined. Unfortunately, the computation of these Green's functions is rather cumbersome and time-consuming when applying a classic procedure. As stated in [14], such a procedure involves an inverse Fourier Transform of a discrete sum of Floquet modes, as follows:

$$G_{A,V}^{\mathrm{per}}(\boldsymbol{\rho}|\boldsymbol{\rho}') = \sum_{m=-\infty}^{+\infty} e^{-j\xi(x-x')} \int_{-\infty}^{+\infty} \tilde{G}_{A,V}^{\mathrm{per}}(\xi, k_y) e^{-jk_y(y-y')} dk_y, \tag{8}$$

with

$$\xi = \frac{\psi}{b} + \frac{2\pi m}{b}. \tag{9}$$

This series (8) converts the well-known spectral Green's functions $\tilde{G}_A^{\mathrm{per}}(\xi, k_y)$ and $\tilde{G}_V^{\mathrm{per}}(\xi, k_y)$ (see [23]) into spatial Green's functions $G_A^{\mathrm{per}}(\boldsymbol{\rho}|\boldsymbol{\rho}')$ and $G_V^{\mathrm{per}}(\boldsymbol{\rho}|\boldsymbol{\rho}')$. No analytical expressions are available for (8). This is due to the presence of the semi-infinite layer of air $z > d$ (Fig. 1). This layer corresponds to a continuous set of radiation modes in the modal spectrum of the microstrip substrate, necessitating the cumbersome, numerical evaluation of Sommerfeld-integrals [24]–[26]. Here, we adopt the PML-paradigm [15], which is detailed in [19] for 1-D periodic layered medium Green's functions. The semi-infinite layer of air above the microstrip substrate is terminated by a PEC plate placed at a *complex* distance $z = d + \mathcal{D}$ (Fig. 3). It can be shown [15] that a proper choice

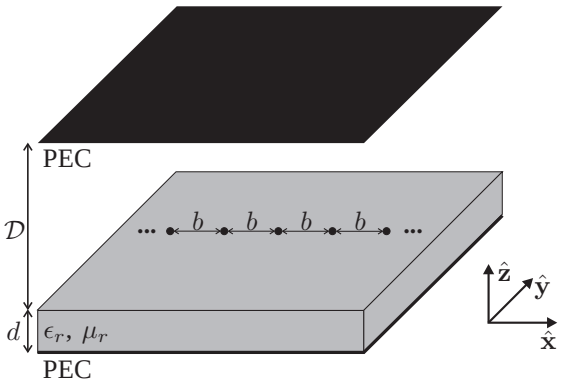

Fig. 3: A 1-D periodic configuration of point sources on the substrate-air interface $z = d$. The air-filled half-space is closed by a PEC-backed PML at complex distance $\mathcal{D}$.

of $\mathcal{D}$ leads to a so-called PML-closed waveguide that very closely mimics the behavior of the original, open waveguide, as the original modal spectrum is now replaced by a *discrete* set of TE- and TM-polarized modes of the PML-closed substrate. Consequently, the Green's functions of the PML-closed waveguide have the interesting property that they can be written as analytical sums of transverse electric (TE) and transverse magnetic (TM) PML-modes. As such, the following expressions for the pertinent spatial 3-D Greens function for a 1-D periodic grid of point sources are obtained:

$$G_A^{\mathrm{per}}(\boldsymbol{\rho}|\boldsymbol{\rho}') = -\frac{j}{2} \sum_{n=1}^{\infty} \sum_{m=-\infty}^{+\infty} \frac{e^{-jm\psi} H_0^{(2)}(\beta_{\mathrm{TE},n}\Delta_m)}{M^{\mathrm{TE}}(\beta_{\mathrm{TE},n})}, \tag{10}$$

$$\begin{aligned} G_V^{\mathrm{per}}(\boldsymbol{\rho}|\boldsymbol{\rho}') = {} & -\frac{j\omega^2}{2} \sum_{n=1}^{\infty} \sum_{m=-\infty}^{+\infty} \frac{e^{-jm\psi} H_0^{(2)}(\beta_{\mathrm{TE},n}\Delta_m)}{\beta_{\mathrm{TE},n}^2 M^{\mathrm{TE}}(\beta_{\mathrm{TE},n})} \\ & - \frac{j}{2} \sum_{n=1}^{\infty} \sum_{m=-\infty}^{+\infty} \frac{e^{-jm\psi} H_0^{(2)}(\beta_{\mathrm{TM},n}\Delta_m)}{\beta_{\mathrm{TM},n}^2 M^{\mathrm{TM}}(\beta_{\mathrm{TM},n})}, \end{aligned} \tag{11}$$

where $\Delta_m = \sqrt{(x-x'-mb)^2 + (y-y')^2}$ and with

$$\begin{aligned} M^{\mathrm{TE}}(\beta) = {} & \frac{d}{\mu_0\mu_r} \frac{1}{\sin^2 \gamma_1 d} - \frac{\cot \gamma_1 d}{\mu_0 \mu_r \gamma_1} \\ & + \frac{\mathcal{D}}{\mu_0} \frac{1}{\sin^2 \gamma_0 \mathcal{D}} - \frac{\cot \gamma_0 \mathcal{D}}{\mu_0 \gamma_0}, \end{aligned} \tag{12}$$

$$\begin{aligned} M^{\mathrm{TM}}(\beta) = {} & \frac{\epsilon_0 \epsilon_r \cot \gamma_1 d}{\gamma_1^3} + \frac{\epsilon_0 \epsilon_r d}{\gamma_1^2 \sin^2 \gamma_1 d} \\ & + \frac{\epsilon_0 \cot \gamma_0 \mathcal{D}}{\gamma_0^3} + \frac{\epsilon_0 \mathcal{D}}{\gamma_0^2 \sin^2 \gamma_0 \mathcal{D}}, \end{aligned} \tag{13}$$

where $\gamma_0 = \sqrt{k_0^2 - \beta^2}$ and $\gamma_1 = \sqrt{k_0^2 \epsilon_r \mu_r - \beta^2}$. In (10) and (11), $H_0^{(2)}(\cdot)$ is the zeroth-order Hankel function of the second kind. Although the summations over the modes n in (10) and (11) have an infinite extent, because of the fact that the modal propagation constants $\beta_{\mathrm{TE},n}$ and $\beta_{\mathrm{TM},n}$ are located in the fourth quadrant of the complex plane, only a limited set of these modes needs to be retained. In all examples

presented below (Section III), less than 100 modes are used. It was explained in [16] that these modes come in three flavors, which exhibit different behavior. The choice of the PML-parameters, i.e., the choice of the complex thickness $\mathcal{D}$, has to be appropriate to provide sufficient damping of the modal fields inside the PML for each of these modes. The influence of $\mathcal{D}$ was also discussed in [27], along with an indicator of the quality of this choice. For large n, the series in (10) and (11) converge at a rate proportional to $e^{-n\,C_1\Delta_m}$, with C_1 a constant. Hence, given this exponential decay as a function of n and provided that the distance Δ_m is not too small, these are fast converging series. For small n or for small distances Δ_m, however, a combination of techniques — such as Poisson summation, Shank's acceleration, and/or Ewald splitting — has to be applied to improve the convergence. A rigorous description of these techniques is outside the scope of this work, but they are described in detail in [19] and the references therein. In summary, it has been shown that the PML-paradigm allows computing layered medium Green's functions, and 1-D periodic layered medium Green's functions in particular, in a very efficient and elegant way, this in contrast to more classical Sommerfeld-approaches. In this paper, for the first time, the PML-based approach is adopted to construct a 1-D periodic BIE-MoM for the analysis of straight and meandering microstrip lines.

III. Numerical examples

The 1-D periodic BIE-MoM technique is now validated and illustrated by considering representative (application) examples. First, the currents induced on a large semi-infinite PEC plate are studied, leading to a validation of the technique. Second, the radiation onto a straight microstrip line is modeled. It is shown that, for straight lines, the period b has no significant influence. Third, a serpentine delay line is investigated and compared to another efficient BIE-MoM technique for large, but finite structures, showing excellent agreement and demonstrating the efficiency of the new periodic technique. All computations are performed using a Linux-based 64-bit AMD Opteron 2350 computer with 32 GB of RAM running at 2 GHz. A BiCGstab iterative scheme [28] was used to solve linear system (5).

A. Semi-infinite plate

As a first example a large PEC plate is considered. The metallization within one unit cell $m = 0$ is shown in Fig. 2 with $b = 5$ mm and $w = 300$ mm. So, the length of the plate along the y-dimension is 10 free-space wavelengths $\lambda_0 = 2\pi/k_0$. The plate has an infinite extent along the x-axis. The metallization resides on a PEC-backed non-magnetic substrate of thickness $d = 3.17$ mm and with relative permittivity $\epsilon_r = 11.7$. The PEC plate is illuminated by a plane wave $\mathbf{E}^{\mathrm{PW}}(\mathbf{r}) = (\hat{\mathbf{x}} + \hat{\mathbf{y}})e^{jk_0 z}\ \frac{\mathrm{V}}{\mathrm{m}}$, i.e. under perpendicular incidence ($\theta = 0°$), and with an angular frequency of $\omega = 2\pi 10$ GHz. The current density on this PEC plate, induced by the plane wave, is computed using the technique described in Section II. The magnitude and the phase of the x- and the y-oriented current densities are shown in Figs. 4 and 5 respectively. In Fig. 6 the magnitude of the x- and the y-oriented current densities is shown along the cross-section $x = (m + 1/2)b = 2.5$ mm. The results are explained as follows. Given the perpendicular incidence of the plane wave, the situation can be considered as a pure 2-D situation, i.e. there is no variation along the x-dimension. In this case, Maxwell's equations can be split into a TE- and a TM-part w.r.t. the x-axis. This was clearly described in [29], where the corresponding 2-D PEC plate was simulated. The results obtained here with the periodic BIE-MoM are exactly the same as those presented in [29]: (i) For the x-oriented current (corresponding to a 2-D TM-solution) the plane wave is completely reflected at the nearly infinitely large PEC plate. Hence, apart from some expected edge effects at $y = 0$ and $y = 10\lambda_0$, the magnitude of the induced currents equals twice the incident x-component of the magnetic field, i.e. $|J_x| = 2\sqrt{\frac{\epsilon_0}{\mu_0}}\ \frac{\mathrm{A}}{\mathrm{m}} = 5.3\ \frac{\mathrm{mA}}{\mathrm{m}}$. (ii) The y-oriented currents can be explained as the currents that correspond to the TEM-wave that is excited inside the parallel-plate waveguide consisting of the PEC ground plate and the PEC metallization, filled with a dielectric. The wavelength of the TEM-wave then equals $\lambda_{\mathrm{TEM}} = \lambda_1 = \lambda_0/\sqrt{\epsilon_r} = 8.77$ mm. This wavelength nicely corresponds to the number of oscillations observed in the y-oriented current.

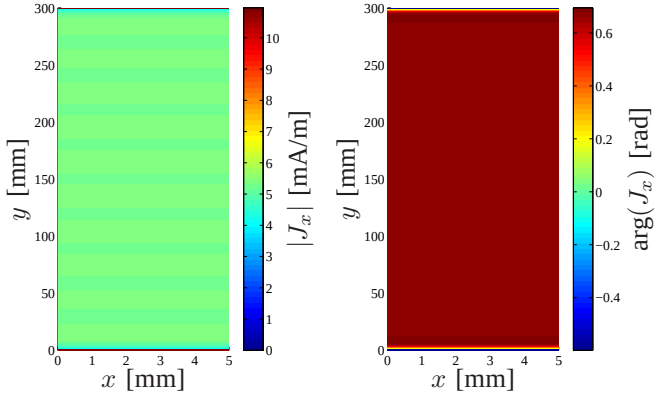

(a) Magnitude (b) Phase

Fig. 4: x-oriented current density J_x on the semi-infinite plate (perpendicular illumination).

In the next example, the same substrate and metallization are used, but the plane wave now impinges obliquely. The angles of incidence are chosen as follows: $\theta = 30°$ and $\phi = 0°$, and hence, the plane wave is defined as $\mathbf{E}^{\mathrm{PW}}(\mathbf{r}) = (\frac{\sqrt{3}}{2}\hat{\mathbf{x}} + \hat{\mathbf{y}} - \frac{1}{2}\hat{\mathbf{z}})e^{jk_0(\frac{1}{2}x + \frac{\sqrt{3}}{2}z)}\ \frac{\mathrm{V}}{\mathrm{m}}$. This situation can no longer be decomposed into a 2-D TM- and TE-problem. There will be a strong coupling between the x- and y-oriented currents, as can be seen in Figs. 7 and 8, and also in Fig. 9 where a cross-section is made along $x = (m + 1/2)b = 2.5$ mm. It is observed from Figs. 7 and 8 that there is no variation of the current density's magnitude along the x-dimension, as expected. There is, however, a variation of its phase. This is clearly illustrated in Fig. 10, where the phase of the x- and the y-oriented current density is shown along the cross-section $y = 5\lambda_0 = 17.1\,\lambda_1 = 150$ mm. This phase varies linearly between $x = 0$ and $x = b$ (from 0.57 rad to 1.09 rad for J_x, and from 0.97 rad to 1.49 rad for J_y). Using (3), it

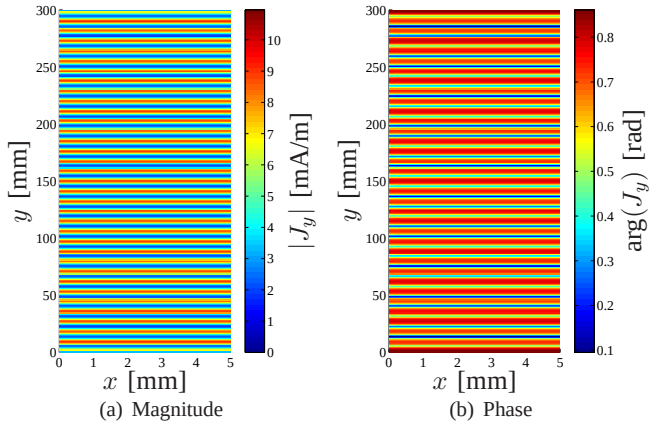

(a) Magnitude (b) Phase

Fig. 5: y-oriented current density J_y on the semi-infinite plate (perpendicular illumination).

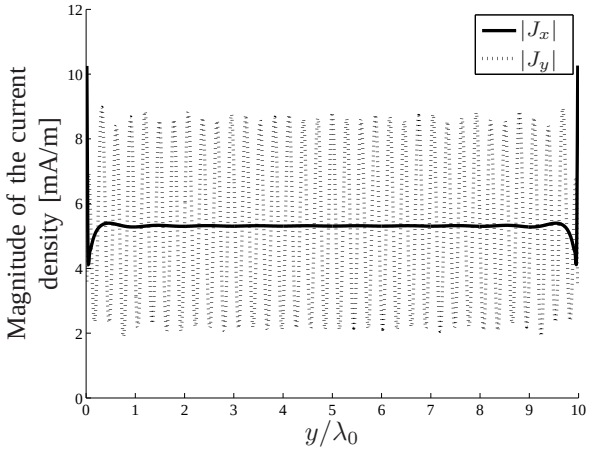

Fig. 6: Magnitude of the x- and the y-oriented current density along $x = (m + 1/2)b = 2.5$ mm on the semi-infinite plate (perpendicular illumination).

is validated that this phase variation of 0.52 rad is in perfect agreement with the predicted value of $\psi = -b\,k_0\,\sin\theta\cos\phi = -0.52$.

The results obtained for this semi-infinite plate validate the proposed 1-D periodic BIE-MoM technique.

B. Straight microstrip line

As an important but simple application example, we consider a straight microstrip line residing on the same substrate as presented above in Section III-A. The metallization within the unit cell is also the one shown in Fig. 2, but now, the width is much smaller, i.e. $w = 4.5$ mm. Again, the plane wave $\mathbf{E}^{\mathrm{PW}}(\mathbf{r}) = (\frac{\sqrt{3}}{2}\hat{\mathbf{x}} + \hat{\mathbf{y}} - \frac{1}{2}\hat{\mathbf{z}})e^{jk_0(\frac{1}{2}x+\frac{\sqrt{3}}{2}z)}\ \frac{\mathrm{V}}{\mathrm{m}}$ with angular frequency $\omega = 2\pi 10$ GHz impinges upon the structure. Although the geometry is invariant w.r.t x-axis, the excitation exhibits a variation of the phase, and hence, this situation cannot be decomposed into a pure 2-D TM- and TE-problem (there is a coupling between the x- and y-oriented currents). For a period $b = 10$ mm, the magnitude of the x- and y-oriented current density along the cross-section $x = b/2 = 5$ mm is presented in Fig. 11. As explained above (Section III-

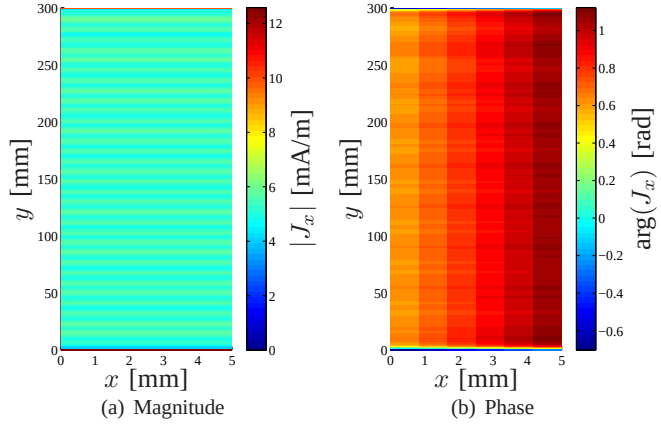

(a) Magnitude (b) Phase

Fig. 7: x-oriented current density J_x on the semi-infinite plate (oblique illumination).

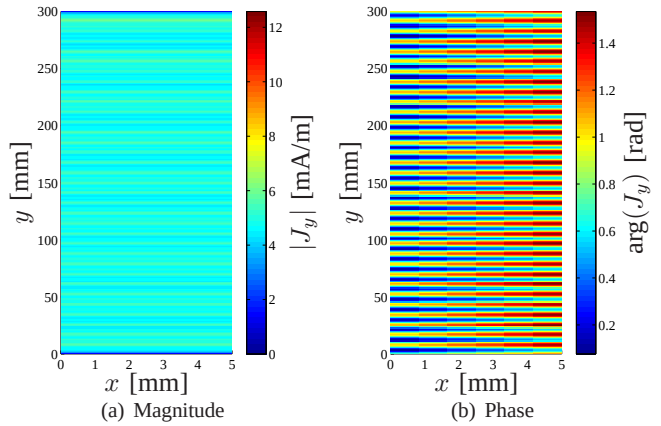

(a) Magnitude (b) Phase

Fig. 8: y-oriented current density J_y on the semi-infinite plate (oblique illumination).

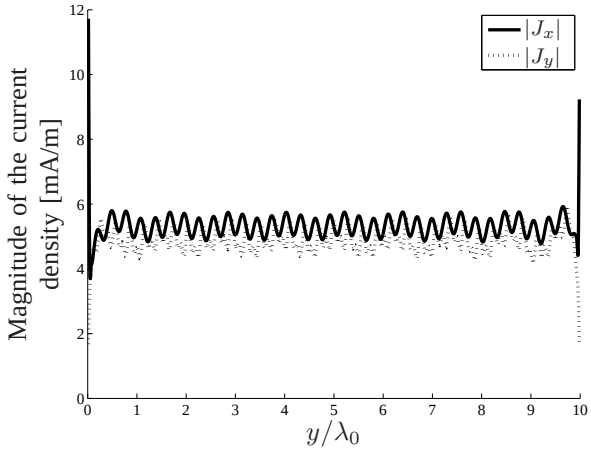

Fig. 9: Magnitude of the x- and the y-oriented current density along $x = (m + 1/2)b = 2.5$ mm on the semi-infinite plate (oblique illumination).

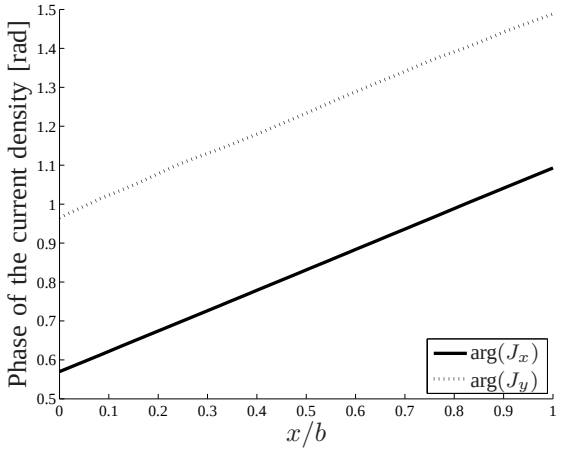

Fig. 10: Phase of the x- and the y-oriented current density along $y = 5\lambda_0 = 17.1\lambda_1 = 150$ mm on the semi-infinite plate (oblique illumination).

A), there is no variation of the magnitude of the current density along the x-direction, but there is, however, a linear variation of its phase. This is clearly illustrated in Fig. 12, where the phase of the x- and the y-oriented current density is shown along the cross-section $y = 2.25$ mm. The phase varies linearly between $x = 0$ and $x = b$ (from 0.06 rad to 1.11 rad for J_x, and from 0.30 rad to 1.35 rad for J_y). Using (3), it is validated that this phase variation of 1.05 rad is in perfect agreement with the predicted value of $\psi = -b\,k_0\,\sin\theta\cos\phi = -1.05$.

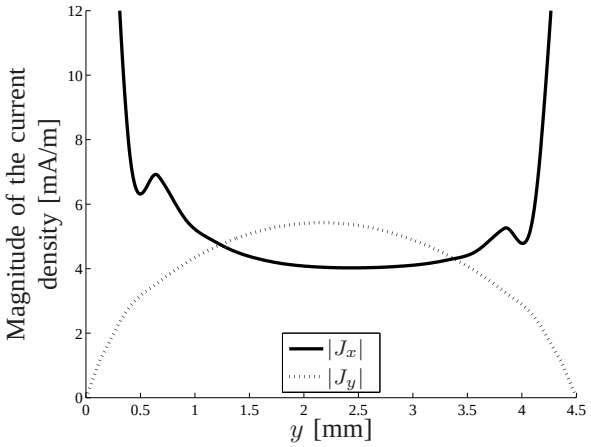

Fig. 11: Magnitude of the x- and the y-oriented current density along $x = b/2 = 5$ mm on the straight microstrip line.

Besides demonstrating, a.o., the linear phase variation of the current density, another interesting way to validate the method is proposed next, using the microstrip example. We simulate the same microstrip configuration, but now for ten different values of the period b, i.e. for b varying from 10 mm to 1 mm in steps of 1 mm. Taking the result of Fig. 11, where $b = b_{\rm ref} = 10$ mm, as a reference result, the relative error between

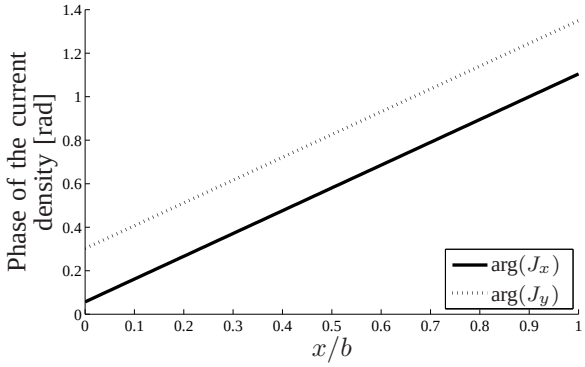

Fig. 12: Phase of the x- and the y-oriented current density along $y = 2.25$ mm on the straight microstrip line.

the magnitude of the current densities is calculated as follows:

$$\delta_x(b) = \left| \frac{\int_0^w |J_x^{\rm ref}(b_{\rm ref}/2, y, d)|\,dy - \int_0^w |J_x^{\rm var}(b/2, y, d)|\,dy}{\int_0^w |J_x^{\rm ref}(b_{\rm ref}/2, y, d)|\,dy} \right|, \tag{14}$$

$$\delta_y(b) = \left| \frac{\int_0^w |J_y^{\rm ref}(b_{\rm ref}/2, y, d)|\,dy - \int_0^w |J_y^{\rm var}(b/2, y, d)|\,dy}{\int_0^w |J_y^{\rm ref}(b_{\rm ref}/2, y, d)|\,dy} \right|, \tag{15}$$

where $J_x^{\rm ref}(b_{\rm ref}/2, y, d)|$ and $J_y^{\rm ref}(b_{\rm ref}/2, y, d)|$ are the reference results presented in Fig. 11, and with $J_x^{\rm var}(b/2, y, d)|$ and $J_y^{\rm var}(b/2, y, d)|$ the current densities obtained for the same microstrip configuration, but using another value for the period b. The relative errors (14) and (15) are shown in Fig. 13. It is observed that reducing the period b yields the same result, at least, within a margin of error that is smaller than 0.01%. Hence, apart from using this result as a validation, it is also clear that for straight configurations, it is beneficial to take b small, as this reduces the number of unknowns N in the MoM. Note, however, that when the number of discretization cells along the x-direction becomes too small, say less than three, this methods breaks down. In the above case for $b = 1$ mm, there are four discretization cells along the x-direction.

C. Serpentine delay line

The last application example, presented in this section, is the serpentine delay line configuration shown in Fig. 1. The PEC metallization within one unit cell, indicating all detailed dimensions, is shown in Fig. 14. This metallization resides on top of a PEC-backed, non-magnetic, lossy substrate of thickness $d = 1.5$ mm, relative permittivity $\epsilon_r = 4.3$, and loss tangent $\tan\delta = 0.02$. A similar serpentine delay line was proposed in [10], where its signal integrity properties were studied. Here, we evaluate the effects of radiation onto the serpentine delay line at an angular frequency of $\omega = 2\pi 20$ GHz by letting a plane wave $\mathbf{E}^{\rm PW}(\mathbf{r}) = (\hat{\mathbf{x}} + \hat{\mathbf{y}} - \sqrt{2}\hat{\mathbf{z}})e^{jk_0(\frac{1}{2}x + \frac{1}{2}y + \frac{\sqrt{2}}{2}z)}\ \frac{\rm V}{\rm m}$ obliquely impinge upon it ($\theta = 45°$ and $\phi = 45°$). The magnitude of the x- and y-oriented current

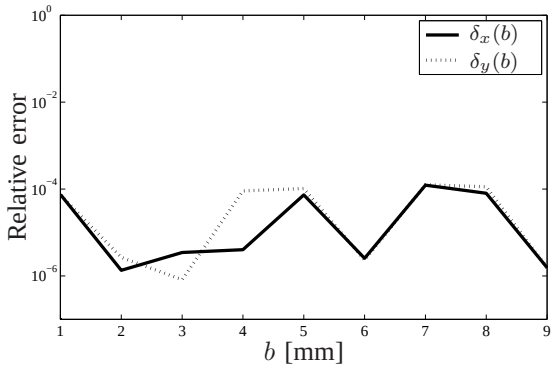

Fig. 13: Relative error on the magnitude of the x- and the y-oriented current density on the straight microstrip line for a varying period b, compared to the situation with $b = 10$ mm.

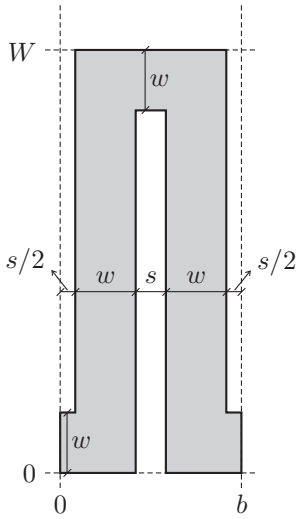

Fig. 14: Metallization of the serpentine delay line within the unit cell $m = 0$. The geometrical parameters are as follows: $b = 9$ mm, $W = 67$ mm, $w = 3$ mm, and $s = 1.5$ mm.

density induced on the unit cell's metallization is shown in Figs. 15(a) and 16(a) respectively. To obtain this result, the 1-D periodic BIE-MoM, presented in this paper, is used. For comparison, a finite serpentine line consisting of seven unit cells and illuminated by the same plane wave, is simulated using the SVD-PML-MLFMA technique [18]. This technique was especially conceived to rapidly analyze large, but *finite*, *non*-periodic structures residing on microstrip substrates. In Figs. 15(b) and 16(b) the magnitude of the x- and the y-oriented induced current density that flows within the center unit cell (i.e. the fourth unit cell) is shown. There is an excellent agreement with the results obtained by the new 1-D periodic BIE-MoM. Of course, increasing the number of unit cells in the SVD-PML-MLFMA further increases the accuracy. The convergence rate as a function of the number of periods depends on the convergence rate of the series (10) and (11), as presented in Section II-C. Furthermore, it takes only 0.55 seconds to perform one matrix-vector multiplication in the iterative solution of the linear system (5) using the 1-D periodic BIE-MoM, leading to the results presented in Figs. 15(a) and 16(a). In contrast, although the matrix-vector multiplications are hugely accelerated by the SVD-PML-MLFMA, it takes 5.57 seconds to perform one matrix-vector multiplication in the iterative solution scheme to achieve the results presented in Fig. 15(b) and 16(b). This speed-up factor of 10.20 is significant and it is of course thanks to the fact that the number of unknowns in the periodic BIE-MoM scheme is rather small, as only one representative unit cell needs to be considered. More specifically, there were $N = 3770$ unknowns in the 1-D periodic BIE-MoM scheme and $N = 26383 \approx 7{\cdot}3770$ in the SVD-PML-MLFMA scheme.

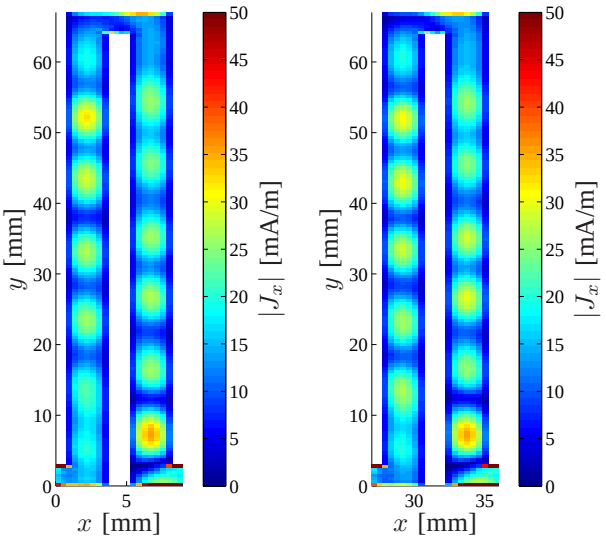

(a) Periodic BIE-MoM (b) SVD-PML-MLFMA

Fig. 15: Magnitude of the x-oriented current density on (a) a unit cell of the serpentine delay line, computed using the 1-D periodic BIE-MoM technique, and (b) the center unit cell of the finite length serpentine delay line consisting of seven unit cells, computed using the SVD-PML-MLFMA [18].

As the analysis can be restricted to one single unit cell, the technique presented here allows a rapid evaluation of the distributed currents induced on (multiconductor) transmission lines, such as straight microstrip lines, coupled microstrip lines, serpentine delay lines, etc. The results can be used for further analysis purposes. Using the Baum-Liu-Tesche (BLT) equation, which was first introduced in [30], for describing (multiconductor) transmission lines, the voltages and currents at loads connected to the lines can be estimated. Also, conjunction with advanced EMI analysis techniques for plane wave excitation [31], or even for near-zone illumination [32], can be investigated. The (application) examples given above validate the presented technique but represent idealized scenarios, using perfect terminations and plane-wave illumination. The extension of the technique to non-perfect terminations of the lines and finite-sized electromagnetic sources is definitely of interest to the EMC/EMI community.

IV. Conclusions

An MPIE is constructed to model the current density induced on 1-D periodic metallizations residing on a microstrip

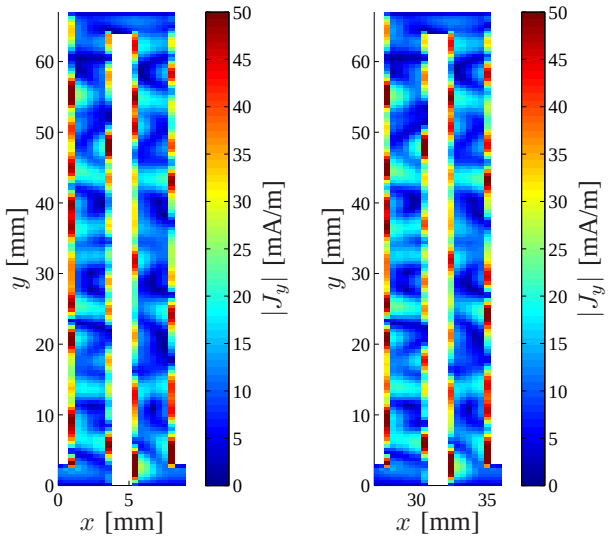

(a) Periodic BIE-MoM (b) SVD-PML-MLFMA

Fig. 16: Magnitude of the y-oriented current density on (a) a unit cell of the serpentine delay line, computed using the 1-D periodic BIE-MoM technique, and (b) the center unit cell of the finite length serpentine delay line consisting of seven unit cells, computed using the SVD-PML-MLFMA [18].

substrate. The periodic structure can be analyzed by merely considering one single representative unit cell, this in accordance with the Floquet-Bloch theorem. Thereto, the pertinent 1-D periodic layered medium Green's functions have to be used. Here, we obtain these Green's function in closed form by invoking the PML-paradigm. The MPIE is solved by means of the MoM. Special attention is devoted to basis functions residing adjacent to the borders of the unit cell, as a continuous current flow across these borders should be guaranteed without destroying the periodicity.

The theory is illustrated by simulating the induced current density onto three different metallizations, illuminated by plane waves, and residing on microstrip substrates. First, the radiation onto a semi-infinite PEC plate is considered. For a perpendicular incidence of the plane wave, it is demonstrated that this situation can be decomposed into a pure 2-D TM- and TE-problem, and the results obtained with the new 1-D periodic BIE-MoM are compared with results from literature. For oblique illumination, it is demonstrated that the phase of the current density varies linearly within the unit cell, as expected from the Floquet-Bloch theorem. Second, the radiation onto a straight microstrip line is modeled. In addition to observing a linear phase variation within the unit cell, it is also shown, by varying the period b, that only a small section of the microstrip line, making up one unit cell, needs to be considered without loosing accuracy (and with a considerable gain in simulation speed). Third, a serpentine delay line is studied. These structures have already been the subject of signal integrity studies, but of course, determination of their susceptibility to electromagnetic radiation is of equal importance. The current density induced onto such a line, which is illuminated by a plane wave obliquely impinging upon it, is accurately simulated and compared to the previously developed (and validated) SVD-PML-MLFMA, showing excellent agreement. Although this SVD-PML-MLFMA was especially constructed to rapidly assess the radiation onto large but finite microstrip structures, the 1-D periodic BIE-MoM is still faster, as only a single unit cell needs to be considered.

REFERENCES

[1] S. Chakravarty and R. Mittra, "Application of the micro-genetic algorithm to the design of spatial filters with frequency-selective surfaces embedded in dielectric media," *IEEE Trans. Electromagn. Compat.*, vol. 44, no. 2, pp. 338–346, May 2002.

[2] C.-N. Chiu, Y.-C. Chang, H.-C. Hsieh, and C. H. Chen, "Suppression of spurious emissions from a spiral inductor through the use of a frequency-selective surface," *IEEE Trans. Electromagn. Compat.*, vol. 52, no. 1, pp. 56–63, Feb. 2010.

[3] M. G. Silveirinha and C. A. Fernandes, "Homogenization of 3-D-connected and nonconnected wire metamaterials," *IEEE Trans. Microw. Theory Tech.*, vol. 53, no. 4, pp. 1418–1430, Apr. 2005.

[4] T.-L. Wu, H.-H. Chuang, and T.-K. Wang, "Overview of power integrity solutions on package and PCB: Decoupling and EGB isolation," *IEEE Trans. Electromagn. Compat.*, vol. 52, no. 2, pp. 346–356, May 2010.

[5] A. C. Scogna, A. Orlandi, and V. Ricchiuti, "Signal and power integrity analysis of differential lines in multilayer printed circuit boards with embedded electromagnetic bandgap structures," *IEEE Trans. Electromagn. Compat.*, vol. 52, no. 2, pp. 357–364, May 2010.

[6] S. Paulotto, P. Baccarelli, F. Frezza, and D. R. Jackson, "A novel technique for open-stopband suppression in 1-D periodic printed leaky-wave antennas," *IEEE Trans. Antennas Propag.*, vol. 57, no. 7, pp. 1894–1906, Jul. 2009.

[7] R. Rodríguez-Berral, F. Mesa, P. Baccarelli, and P. Burghignoli, "Fast numerical analysis of a 1D array of microstrip patches," in *Proceedings of the 2007 IEEE Antennas and Propagation Society International Symposium*, vol. 1–12, Honolulu, HI, USA, 9-15 June 2007, pp. 1677–1680.

[8] G. Lovat, P. Burghignoli, and S. Celozzi, "Shielding properties of a wire-medium screen," *IEEE Trans. Electromagn. Compat.*, vol. 50, no. 1, pp. 80–88, Feb. 2008.

[9] B. Huyghe, H. Rogier, J. Vanfleteren, and F. Axisa, "Design and manufacturing of stretchable high-frequency interconnects," *IEEE Trans. on Advanced Packaging*, vol. 31, no. 4, pp. 802–808, Nov. 2008.

[10] G.-H. Schiue, C.-Y. Chao, W.-D. Guo, and R.-B. Wu, "Improvements of time-domain transmission waveform in serpentine delay line with guard traces," in *IEEE International Symposium on EMC: Workshop and Tutorial Notes*, vol. 1–3, Honolulu, HI, USA, 2007, pp. 754–758.

[11] R. F. Harrington, *Field computation by moment methods.* Piscataway, NJ: IEEE Press, 1993.

[12] D. Vande Ginste, H. Rogier, and D. De Zutter, "Scattering and radiation from/by 1-D periodic metallizations residing in layered media," *IEEE Transactions on Antennas and Propagation*, vol. 58, no. 10, pp. 3316–3326, Oct. 2010.

[13] S. Li, D. Van Orden, and V. Lomakin, "Fast periodic interpolation method for periodic unit cell problems," *IEEE Trans. Antennas Propag.*, vol. 58, no. 12, pp. 4005–4014, Dec. 2010.

[14] P. Baccarelli, C. Di Nallo, S. Paulotto, and D. R. Jackson, "A full-wave numerical approach for modal analysis of 1-D periodic microstrip structures," *IEEE Trans. Microw. Theory Tech.*, vol. 54, no. 4, pp. 1350–1362, Apr. 2006.

[15] F. Olyslager, "Discretization of continuous spectra based on perfectly matched layers," *SIAM J. Appl. Math.*, vol. 64, no. 4, pp. 1408–1433, May 2004.

[16] D. Vande Ginste, E. Michielssen, F. Olyslager, and D. De Zutter, "An efficient perfectly matched layer based multilevel fast multipole algorithm for large planar microwave structures," *IEEE Trans. Antennas Propag.*, vol. 54, no. 5, pp. 1538–1548, May 2006.

[17] D. Vande Ginste, L. Knockaert, and D. De Zutter, "Error control in the perfectly matched layer based multilevel fast multipole algorithm," *Journal of Computational Physics*, vol. 228, no. 13, pp. 4811–4822, July 2009.

[18] D. Vande Ginste, E. Michielssen, F. Olyslager, and D. De Zutter, "A high-performance upgrade of the perfectly matched layer multilevel fast multipole algorithm for large planar microwave structures," *IEEE Transactions on Antennas and Propagation*, vol. 57, no. 6, pp. 1728–1739, June 2009.

[19] H. Rogier, "New series expansions for the 3D Green's function of multilayered media with 1D periodicity based on perfectly matched layers," *IEEE Trans. Microw. Theory Tech.*, vol. 55, no. 8, pp. 1730–1738, Aug. 2007.

[20] J. Sercu, N. Faché, F. Libbrecht, and P. Lagasse, "Mixed potential integral equation technique for hybrid microstrip-slotline multilayered circuits using a mixed rectangular-triangular mesh," *IEEE Trans. Microw. Theory Tech.*, vol. 43, no. 5, pp. 1162–1172, May 1995.

[21] H. Rogier, B. Baekelandt, F. Olyslager, and D. De Zutter, "The FE-BIE technique applied to some 2-D problems relevant to electromagnetic compatibility: Optimal choice of mechanisms to take into account periodicity," *IEEE Trans. Electromagn. Compat.*, vol. 42, no. 3, pp. 246–256, Aug. 2000.

[22] J. Van Bladel, *Electromagnetic Fields*, 2nd ed. Piscataway, NJ, USA: IEEE Press, 2007.

[23] K. A. Michalski and D. Zheng, "Electromagnetic scattering and radiation by surfaces of arbitrary shape in layered media, Part I: Theory," *IEEE Trans. Antennas Propag.*, vol. 38, no. 3, pp. 335–344, March 1990.

[24] L. B. Felsen and N. Marcuvitz, *Radiation and scattering of waves*. Piscataway: IEEE Press, 1994.

[25] N. Faché, F. Olyslager, and D. De Zutter, *Electromagnetic and Circuit Modelling of Multiconductor Transmission Lines*. New York: Oxford University Press Inc., 1993.

[26] F. Olyslager, *Electromagnetic waveguides and transmission lines*. New York: Oxford University Press Inc., 1999.

[27] F. Olyslager and H. Derudder, "Series representation of Green dyadics for layered media using PMLs," *IEEE Trans. Antennas Propag.*, vol. 51, no. 9, pp. 2319–2326, Sept. 2003.

[28] O. Axelsson, *Iterative Solution Methods*. New York: Cambridge University Press, 1994.

[29] D. Vande Ginste, H. Rogier, D. De Zutter, and F. Olyslager, "A fast multipole method for layered media based on the application of perfectly matched layers — the 2-D case," *IEEE Trans. Antennas Propag.*, vol. 52, no. 10, pp. 2631–2640, Oct. 2004.

[30] C. E. Baum, T. K. Liu, and F. M. Tesche, "On the analysis of general multiconductor transmission line networks," *Kirtland AFB, Albuquerque, NM, Interaction Note 350*, 1978.

[31] Y. Bayram and J. L. Volakis, "Hybrid S-parameters for transmission line networks with linear/nonlinear load terminations subject to arbitrary excitations," *IEEE Trans. Microw. Theory Tech.*, vol. 55, no. 5, pp. 941–950, May 2007.

[32] Z. Khan, Y. Bayram, and J. L. Volakis, "EMI/EMC analysis of printed circuit boards subject to near-zone illuminations," *IEEE Trans. Electromagn. Compat.*, vol. 51, no. 2, pp. 406–408, May 2009.